Angewandte Chemie

Supporting Information

Conjugated Copolymers That Shouldn't Be

Jun Guan, Zejun Sun, Ramin Ansari, Yujia Liu, Aimi Endo, Masafumi Unno, Armelle Ouali, Shahrea Mahbub, Joseph C. Furgal, Nuttapon Yodsin, Siriporn Jungsuttiwong, Daniel Hashemi, John Kieffer, and Richard M. Laine*

anie_202014932_sm_miscellaneous_information.pdf

Author Contributions

J.G. Conceptualization: Equal; Data curation: Equal; Formal analysis: Equal; Writing—original draft: Equal; Writing—review & editing: Equal.

SUPPORTING INFORMATION

Table of Contents

Experimental Procedures

Materials. All commercially available chemicals were used as received unless otherwise indicated. Bis(tri-tert-butylphosphine)palladium(0) Pd[P(t-Bu$_3$)]$_2$, N,N-dicyclohexylmethylamine NCy$_2$Me, 1,4-dibromobenzene, 4,4'-dibromo-1,1'-biphenyl, 4,4''-dibromo-p-terphenyl, 4,4'-dibromo-$trans$-stilbene, 2,7-dibromo-9,9-dimethylfluorene, 2,5-dibromothiophene, 5,5'-dibromo-2,2'-bithiophene, 2,5-dibromothieno[3,2-b]thiophene, 2,3,5,6-tetrafluoro-7,7,8,8-tetracyanoquinodimethane F$_4$TCNQ were purchased from Sigma-Aldrich. THF were distilled from over sodium/benzophenone ketyl. Bromine, Br$_2$, zinc dust and glacial acetic acid were purchased from Fisher Scientific. Ladder silsesquioxane vinyl(Me/Ph)Si(O$_{0.5}$)$_2$[PhSiO$_{1.5}$]$_4$(O$_{0.5}$)$_2$Si(Me/Ph)vinyl was a gift from Unno group.

General Heck polymerization of vinyl-LL-vinyl with Br-Ar-Br.[1] To a dry 50 ml Schlenk flask under N$_2$ were added vinyl-LL-vinyl (0.8 mmol), NCy$_2$Me (0.4 g, 2.0 mmol), Br-Ar-Br (0.8 mmol), followed by 30 mL of distilled THF and Pd[P(t-Bu$_3$)]$_2$ (38.7 mg, 0.08 mmol). The mixture was stirred magnetically at 70 °C for 7 d and tracked by GPC. The reaction was quenched by filtering through 1 cm celite which was washed with THF (5 mL). The solution was then concentrated and precipitated into 100 ml cold, well-stirred methanol (yield: 70%). The precipitated product was further purified by column chromatography (silica, 1:1 DCM:hexane). Analytical data are presented in Table **S1-3**.

General bromination of DD-co-phenyl and LL(Me)-co-phenyl.[2] To a dry 100 mL Schlenk flask under N$_2$ were added DD-co-phenyl or LL-co-phenyl (DD/LL SQ: 1.0 mmol), 20 mL of CH$_2$Cl$_2$ and NCy$_2$Me (4.0 mmol). After completely dissolving, Br$_2$ (4.0 mmol) was added dropwise, and an additional 5 ml of CH$_2$Cl$_2$ was added to wash. Thereafter, a vent to a bubbler containing aqueous base was added, and the solution was stirred magnetically at room temperature for 1 d. At this point, 10 g of Na$_2$S$_2$O$_5$ and 5 g of Na$_2$CO$_3$ were dissolved in 40 ml of water and then added to the solution with vigorous stirring until the Br$_2$ color disappeared. The mixture was then transferred to a separatory funnel, and the organic layer was extracted and washed sequentially with 20 ml brine. Thereafter, the organic layer was dried over MgSO$_4$. Then celite was added and stirred for 10 min. The mixture was filtered to give a clear, colorless liquid. Most solvent was removed by rotary evaporation, and the resulting solid was redissolved in a minimal amount of THF and slowly poured into 150 ml cold, well-stirred methanol to fully precipitate the white product (yield: 80%).

General zinc debromination of brominated DD-co-phenyl and LL(Me)-co-phenyl.[3] To a dry 100 mL Schlenk flask under N$_2$ were added above brominated DD-co-phenyl or LL-co-phenyl (DD/LL SQ: 0.8 mmol), 20 mL of diethyl ether, followed by 3 drops of glacial acetic acid and Zn dust (2.0 mmol). The mixture was stirred vigorously under N$_2$ at room temperature. After the grey Zn dust turned into white ZnBr$_2$ powder, the reaction mixture was then filtered. The resulting filtrate was concentrated and precipitated into 100 ml cold, well-stirred methanol to give the yellowish product (yield 65%).

Analytical methods

Matrix-assisted laser desorption/time-of-flight spectrometry. MALDI-TOF was done on a Micromass TOF Spec-2E equipped with a 337 nm nitrogen laser in positive-ion reflectron mode using poly(ethylene glycol) as calibration standard, dithranol as matrix, and $AgNO_3$ as ion source. Samples were prepared by mixing solutions of 5 parts matrix (10 mg/mL in THF), 5 parts sample (1 mg/mL in THF), and 1 part $AgNO_3$ (2.5 mg/mL in THF) and blotting the mixture on target plate.

Nuclear Magnetic Resonance. All ^1H NMR spectra were collected from samples dissolved in $CDCl_3$ and recorded on a Varian INOVA 400 MHz spectrometer. All ^{13}C and 29Si spectra were collected from samples dissolved in CDCl3 and recorded on an Ytterbium 700 MHz. ^1H NMR spectra were collected at 400 MHz using a spectral width of 6000 Hz, a relaxation delay of 0.5 s, 30k data points, a pulse width of 38°, and $CHCl_3$ (7.24 ppm) as the internal reference. ^{13}C NMR spectra were collected at 100 MHz using a 25000 Hz spectral width, a relaxation delay of 1.5 s, 75k data points, a pulse width of 40°. ^{29}Si NMR spectra were collected at 100 MHz using a 14000 Hz spectral width, a relaxation delay of 20 s, 65k data points, a pulse width of 7°.

Gel permeation chromatography. GPC analyses were done on a Waters 440 system equipped with Waters Styragel columns (7.8300, HT 0.5, 2, 3, 4) with RI detection using Waters refractometer and THF as solvent. The system was calibrated using polystyrene.

Thermogravimetric analyses. TGAs were run on a SDT Q600 Simultaneous Differential DTA-TGA Instrument (TA Instruments, Inc., New Castle, DE). Samples (15–20 mg) were loaded in alumina pans and ramped at 10 °C/min to 1000 °C under dry air with a flow rate of 60 mL/min.

Fourier-Transform Infrared Spectroscopy. Diffuse reflectance Fourier transform (DRIFT) spectra were recorded on a Nicolet 6700 Series FTIR spectrometer (Thermo Fisher Scientific, Inc., Madison, WI). Optical grade, random cuttings of KBr (International Crystal Laboratories, Garfield, NJ) were ground, with 1.0 wt % of the sample to be analyzed. For DRIFT analyses, samples were packed firmly and leveled off at the upper edge to provide a smooth surface. The FTIR sample chamber was flushed continuously with N_2 prior to data acquisition in the range 4000−400 cm^{-1} with a precision of ±4 cm^{-1}.

Photophysical characterization.

UV−Vis Spectrometry. UV−vis measurements were recorded on a Shimadzu UV-1601 UV−vis transmission spectrometer. Samples were dissolved in CH_2Cl_2 and diluted to a concentration ($10^{-3}−10^{-4}$ M) where the absorption maximum was <10% for a 1 cm path length.

Photoluminescence spectrometry. Photoluminescent spectra were recorded on a Fluoromax-2 fluorometer in the required solvent using 300 nm excitation. Samples from UV−vis spectroscopy were diluted ($10^{-5}−10^{-6}$ M) to avoid excimer formation and fluorometer detector saturation.

Modeling. Two approaches were assessed:

(1) Ground state optimized structures of all structures were determined using DFT at the B3LYP/6-31G(d,p) level of theory with GD3BJ dispersion correction. The vertical excitation energies and electronic absorption spectra were investigated using time dependent density functional theory (TD-DFT) with hybrid exchange-correlation functionals CAM-B3LYP. All calculations were run with Gaussian 16 program package.

(2). Crystal state calculations were performed using plane-wave DFT within the framework of non spin-polarized density functional theory using the Vienna ab initio simulation package (VASP).[4,5] The exchange-correlation energy and potential are described by Perdew, Burke and Ernzerhof (PBE) potentials.[6] The electronion interaction is described by the projector-augmented wave (PAW) scheme.[7,8] The many body dispersion method of Tkatchenko et al.[9] is used to account for van der Waals interactions. Van der Waals interactions has a huge impact on the electronic properties of double-decker copolymers, since the molecules and different functional groups in the same molecule are very close to one another. The Brillouin zones are sampled using the Gamma point. The convergence with respect to the size of k-sampling and cutoff radius was checked as well. The structures and charge densities were visualized using VESTA program.[10]

Results and Discussion

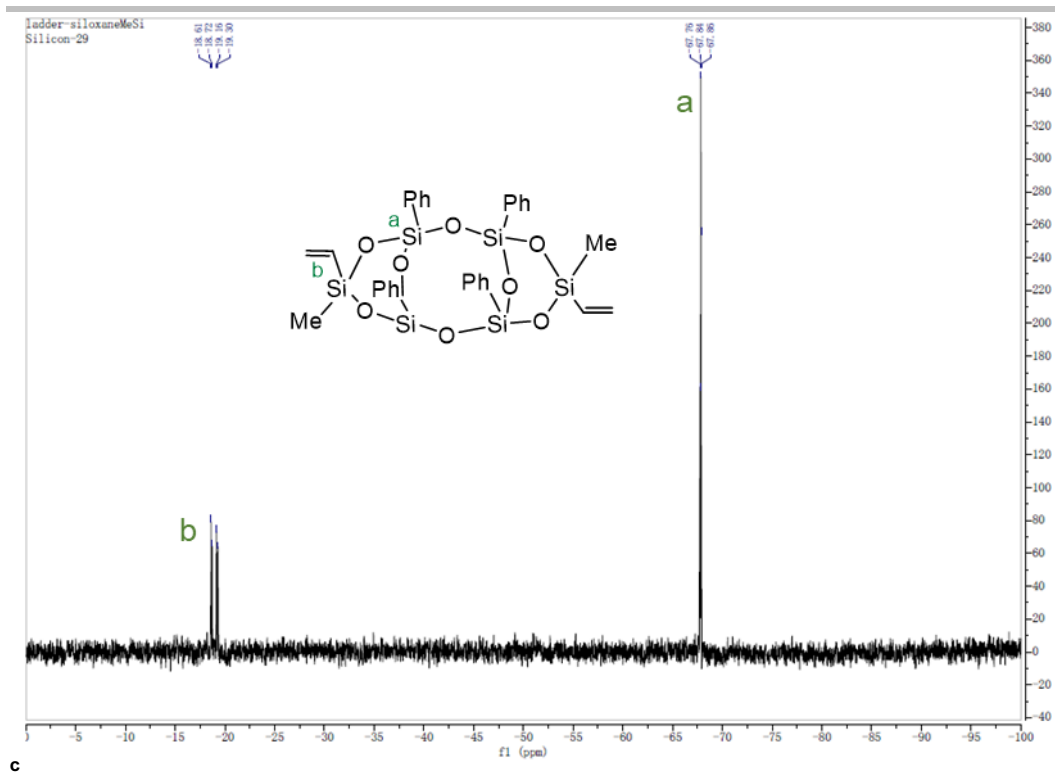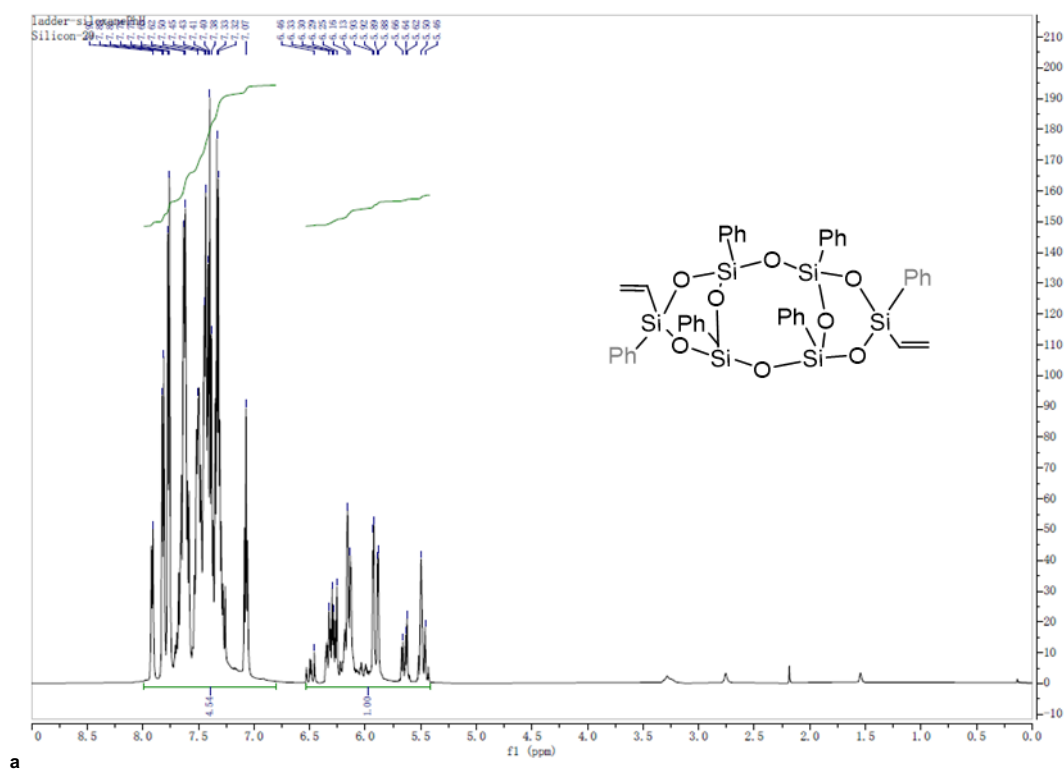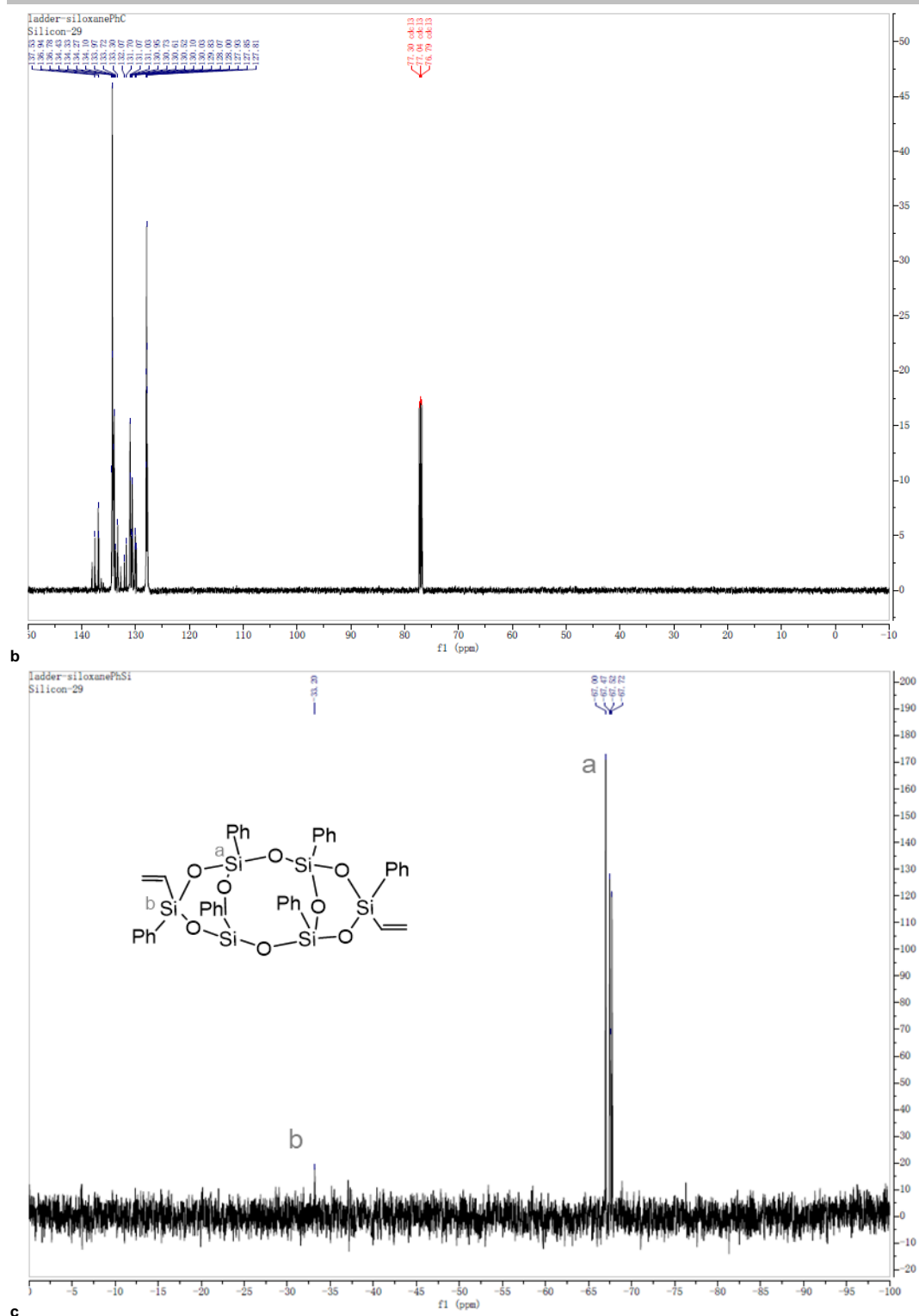Analytical characterization of vinyl-LL-vinyl and derived copolymers.

a

b

4

c

Figure S1. (a) ¹H NMR, (b) ¹³C NMR, (c) ²⁹Si NMR of vinyl-LL(Me)-vinyl.

a

Figure S2. (a) ^{1}H NMR, (b) ^{13}C NMR, (c) ^{29}Si NMR of vinyl-LL(Ph)-vinyl.
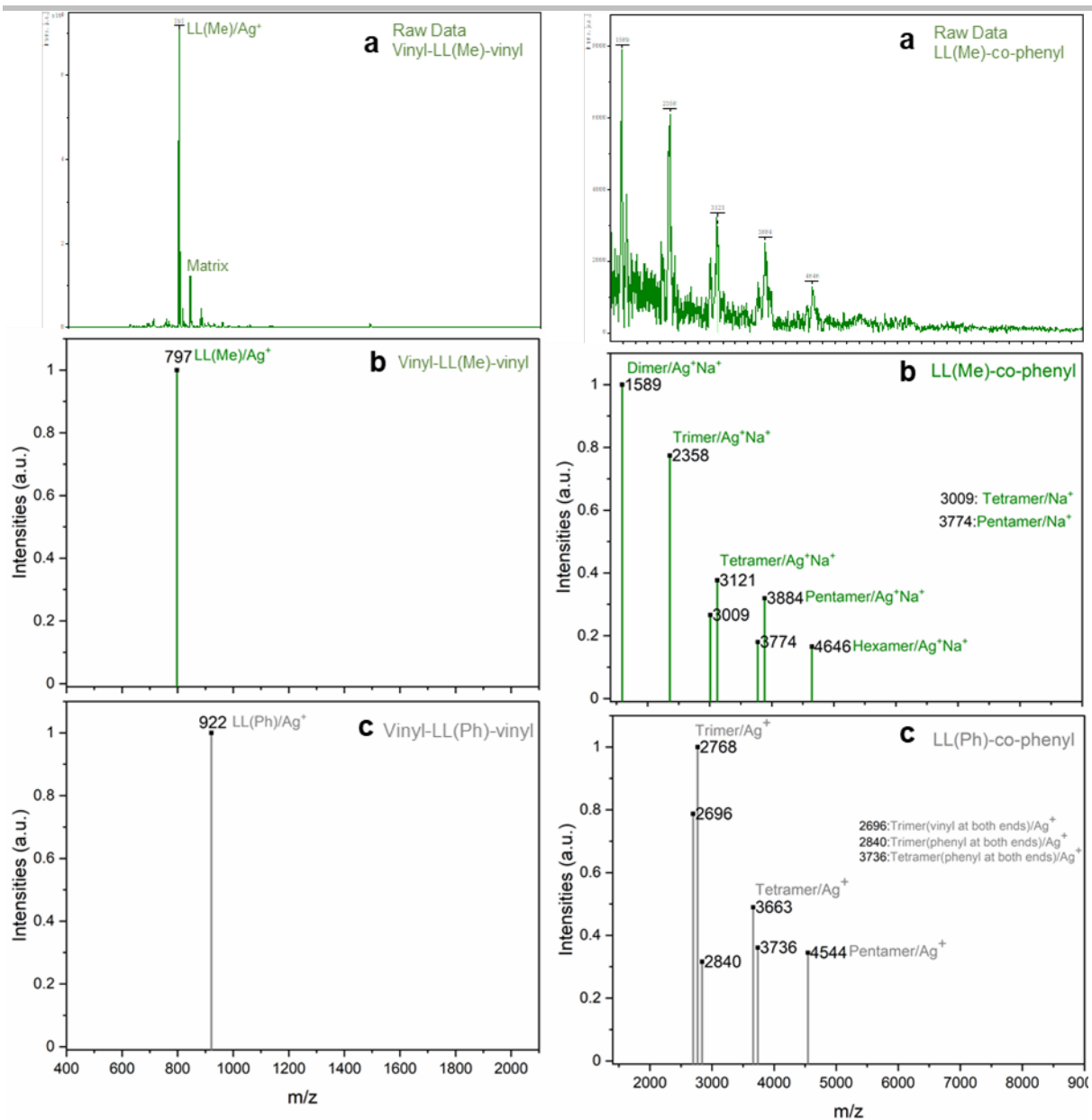
Figure S3. Left: (a) Raw MALDI-TOF of vinyl-LL(Me)-vinyl, (b) Modified MALDI-TOF of vinyl-LL(Me)-vinyl, (c) Modified MALDI-TOF of vinyl-LL(Ph)-vinyl. Right: (a) Raw MALDI-TOF of LL(Me)-co-phenyl, (b) Modified MALDI-TOF of LL(Me)-co-phenyl, (c) Modified MALDI-TOF of LL(Ph)-co-phenyl.
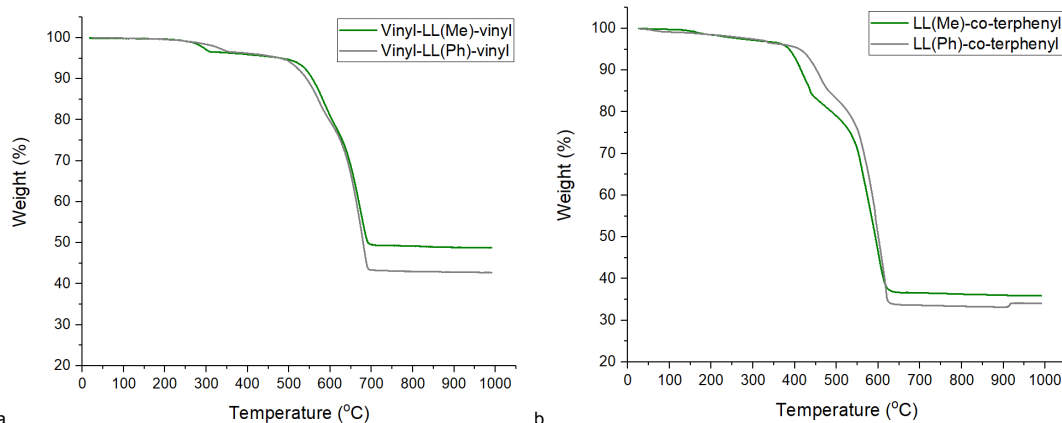
Figure S4. (a) TGA of vinyl-LL(Me)-vinyl and vinyl-LL(Ph)-vinyl, (b) TGA of LL(Me)-co-terphenyl and LL(Ph)-co-phenyl.

SUPPORTING INFORMATION

Table S1. MALDI-TOF, GPC and TGA data for vinyl-LL-vinyl and derived polymers.

Compound	MALDI-TOF m/z		GPC			TGA		
	Mer	Theor	M_n	M_w	Đ[b]	Ceramic yield %	Theor yield %	$T_{d5\%}$ °C (air)
Vinyl-LL(Me)-vinyl	797[a]	797[a]	490	530	1.08	49	51	490
Co-phenyl	764	765	5420	15190	2.80	46	46	430
Co-biphenyl	839	841	11700	44000	3.78	42	42	410
Co-terphenyl	921	917	15850	46580	2.95	37	39	390
Co-stilbene	870	867	6280	19620	3.12	40	41	340
Co-dimethylfluorene	881	881	5810	15780	2.72	39	40	400
Co-thiophene	772	771	3170	6190	1.95	46	46	450
Co-bithiophene	853	853	5540	11330	2.05	40	42	440
Co-thienothiophene	831	827	7400	17100	2.31	41	43	390
Vinyl-LL(Ph)-vinyl	922[a]	921[a]	540	620	1.15	43	43	490
Co-phenyl	891	889	5690	15000	2.63	40	40	430
Co-biphenyl	963	965	8180	28050	3.43	35	37	380
Co-terphenyl	1041	1041	8390	22070	2.63	34	34	420
Co-stilbene	988	991	6620	15990	2.42	35	36	390
Co-dimethylfluorene	1006	1005	5950	17770	2.99	34	35	400
Co-thiophene	895	895	4360	8060	1.85	38	40	400
Co-bithiophene	979	977	4330	6710	1.55	36	36	460
Co-thienothiophene	952	951	7470	19410	2.60	35	37	440

[a] As Ag^{+} adduct. [b] Polydispersity.

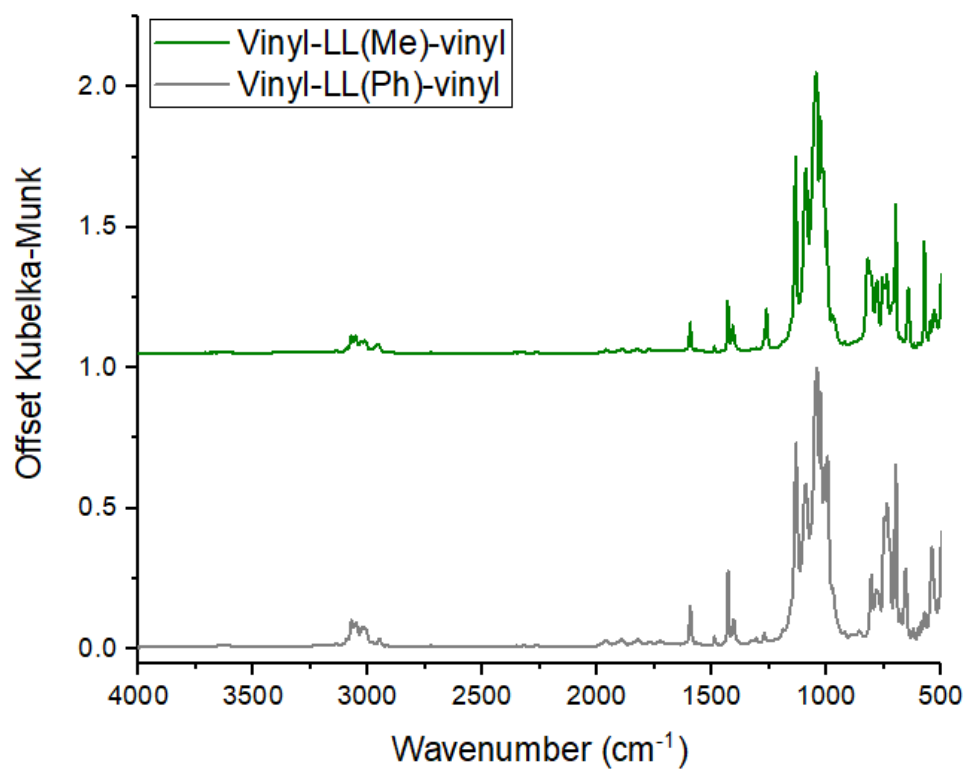**Figure S5.** FTIR of vinyl-LL(Me)-vinyl and vinyl-LL(Ph)-vinyl.

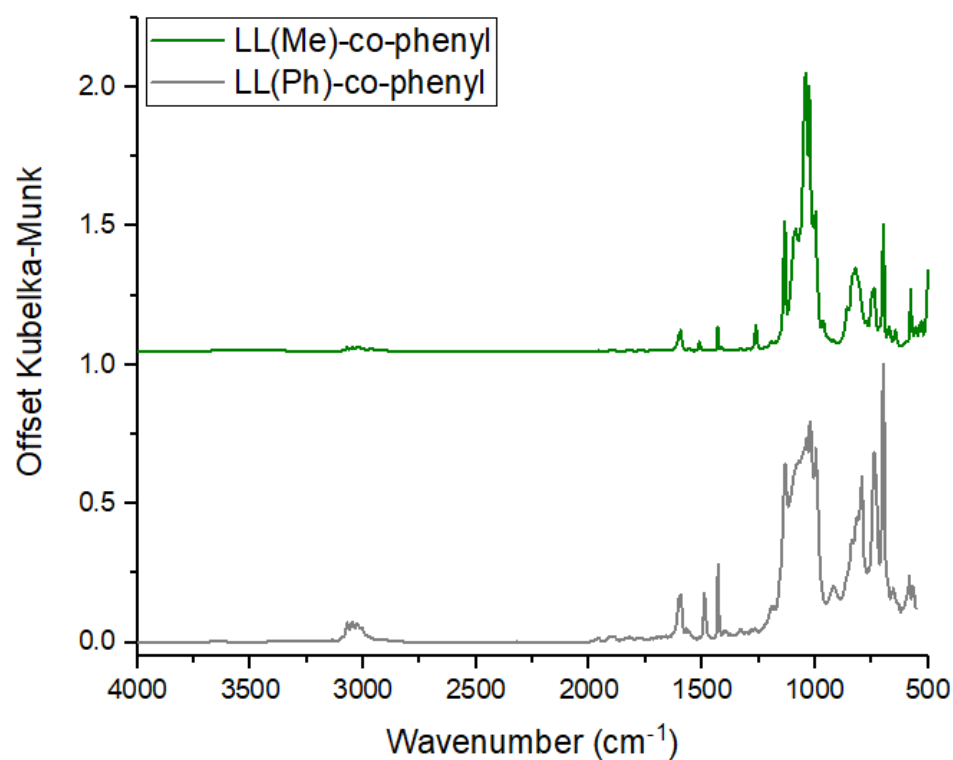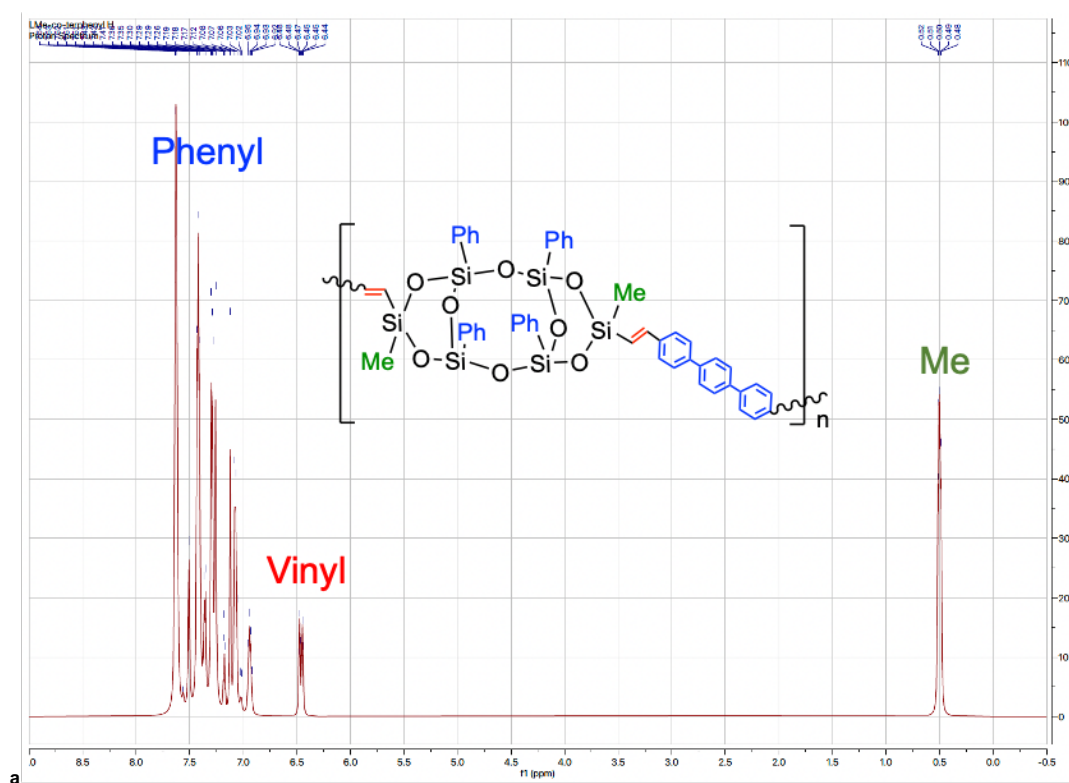**Figure S6.** FTIR of LL(Me)-co-phenyl and LL(Ph)-co-phenyl.

Table S2. Representative FTIR data of selected compounds.

Compound	v	Wavenumber (cm^{-1})	Intensity
Vinyl-LL(Me)-vinyl	Si-O-Si	998	Medium, sharp
	Si-O-Si	1027	Strong, sharp
	Si-O-Si	1044	Strong, sharp
	Si-O-Si	1090	Strong, sharp
	Si-O-Si	1134	Strong, sharp
	C=C	1262	Medium, sharp
	C=C	1408	Weak, sharp
	C=C	1431	Medium, sharp
	C=C	1595	Medium, sharp
	C-H	2950	Weak, broad
	C-H	3073	Weak, broad
LL(Me)-co-phenyl	Si-O-Si	998	Medium, sharp
	Si-O-Si	1026	Strong, sharp
	Si-O-Si	1041	Strong, sharp
	Si-O-Si	1086	Medium, sharp
	Si-O-Si	1135	Medium, sharp
	C=C	1262	Medium, sharp
	C=C	1430	Medium, sharp
	C=C	1595	Medium, sharp
	C-H	3070	Weak, broad
Vinyl-LL(Ph)-vinyl	Si-O-Si	996	Medium, sharp
	Si-O-Si	1026	Strong, sharp
	Si-O-Si	1042	Strong, sharp
	Si-O-Si	1091	Medium, sharp
	Si-O-Si	1134	Strong, sharp
	C=C	1405	Weak, sharp
	C=C	1430	Medium, sharp
	C=C	1594	Medium, sharp
	C-H	2925	Weak, broad
	C-H	3072	Weak, broad
LL(Ph)-co-phenyl	Si-O-Si	996	Strong, sharp
	Si-O-Si	1022	Strong, sharp
	Si-O-Si	1037	Strong, broad
	Si-O-Si	1133	Strong, sharp
	C=C	1429	Medium, sharp
	C=C	1490	Medium, sharp
	C=C	1594	Medium, sharp
	C-H	2925	Weak, broad
	C-H	3049	Weak, broad

b

Figure S7. (a) ^{1}H NMR, (b) ^{13}C NMR of LL(Me)-co-terphenyl.

a

Figure S8. (a) ^{1}H NMR, (b) ^{13}C NMR of LL(Me)-co-thiophene.

Table S3. ^{1}H and [13]NMR data of vinyl-LL(Me)-vinyl derived polymers.

Compound	^{1}H NMR peaks (ppm)	13C NMR peaks (ppm)
LL-co-phenyl	7.7-7.2 (m, 20H, cage-Ph); 7.2-7.0 (m, 4H, co-Ph); 6.9 (d, 2H, vinyl); 6.5 (d, 2H, vinyl); 0.5 (m, 6H, Me)	146.1; 137.8; 134.0; 132.0; 131.1; 127.7; 127.0; 124.2; -0.6
LL-co-biphenyl	7.6-7.2 (m, 20H, Ph); 7.2-7.0 (m, 8H, Ph); 6.9 (d, 2H, vinyl); 6.5 (d, 2H, vinyl); 0.4 (m, 6H, Me)	146.1; 140.6; 136.7; 134.2; 132.0; 130.8 127.8; 126.9; 124.3; -0.7
LL-co-terphenyl	7.7-7.3 (m, 20H, Ph); 7.3-7.0 (m, 12H, Ph); 7.0 (d, 2H, vinyl); 6.5 (d, 2H, vinyl); 0.5 (m, 6H, Me)	146.1; 140.5; 139.8; 136.8; 134.2; 132.0; 130.7; 127.9; 127.0; 124.3; -0.7
LL-co-stilbene	7.8-7.0 (m, 28H, Ph); 6.9 (m, 3H, vinyl); 6.4 (m, 3H, vinyl); 0.5 (t, 6H, Me)	146.2; 137.7; 137.5; 136.1 134.0; 132.0; 131.1; 127.9; 127.0; 124.3; -0.6
LL-co-dimethylfluorene	8.0-7.2 (m, 26H); 7.0 (d, 2H, vinyl); 6.5 (d, 2H, vinyl); 1.8 (s, 6H, Me); 0.4 (m, 6H, Me)	147.8; 146.2; 141.0; 137.7; 134.0; 131.9; 130.8; 129.6; 127.6; 126.7; 123.2; 121.6; 45.5; 30.9; -0.6;
LL-co-thiophene	7.6-7.1 (m, 22H); 6.9 (d, 2H, vinyl); 6.4 (d, 2H, vinyl); 6.2 (t, 2H, vinyl); 6.0 (q, 1H, vinyl); 0.5 (m, 6H, Me)	144.2; 139.1; 134.4; 134.0; 131.9; 130.4; 127.8; 127.5; 124.0; -0.7
LL-co-bithiophene	7.7-7.2 (m, 24H); 6.9 (d, 2H, vinyl); 6.5 (d, 2H, vinyl); 6.2 (t, 2H, vinyl); 5.9 (q, 1H, vinyl); 0.5 (m, 6H, Me)	144.2; 139.1; 138.1; 134.1; 134.0; 132.5; 131.8; 130.4; 127.7; 127.5; 124.0; -0.6
LL-co-thienothiophene	7.6-7.2 (m, 22H); 6.9 (d, 2H, vinyl); 6.5 (d, 2H, vinyl); 6.2 (t, 2H, vinyl); 5.9 (m, 1H, vinyl); 0.5 (m, 6H, Me)	144.1; 139.1; 134.4; 133.9; 131.8; 130.3; 129.3; 127.7; 127.5; 124.0; -0.6

Photophysical characterization of vinyl-LL-vinyl and derived copolymers.

Figure S9. Normalized steady-state spectra of 4,4'-[(MeO)$_2$Sivinyl]$_2$biphenyl, DD-co-biphenyl and LL(Me/Ph)-co-biphenyl in CH$_2$Cl$_2$.
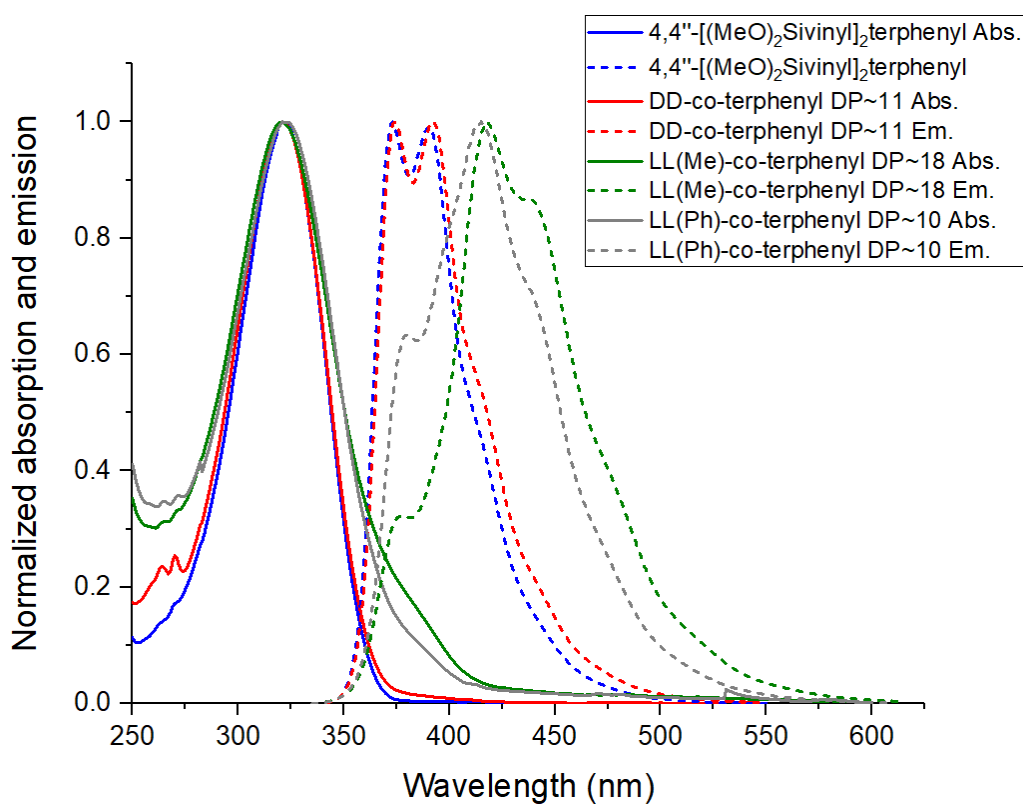

Figure S10. Normalized steady-state spectra of 4,4''-[(MeO)$_2$Sivinyl]$_2$terphenyl, DD-co-terphenyl and LL(Me/Ph)-co-terphenyl in CH$_2$Cl$_2$.
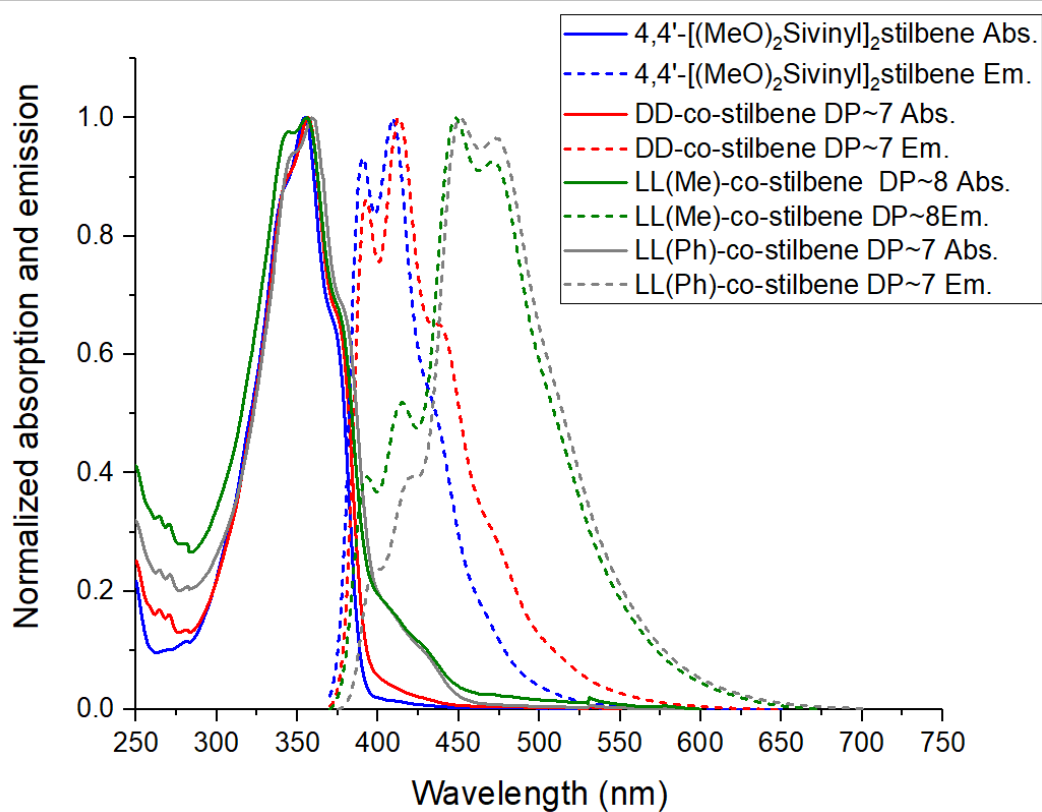
Figure S11. Normalized steady-state spectra of 4,4'-[(MeO)$_2$Sivinyl]$_2$stilbene, DD-co-stilbene and LL(Me/Ph)-co-stilbene in CH$_2$Cl$_2$.
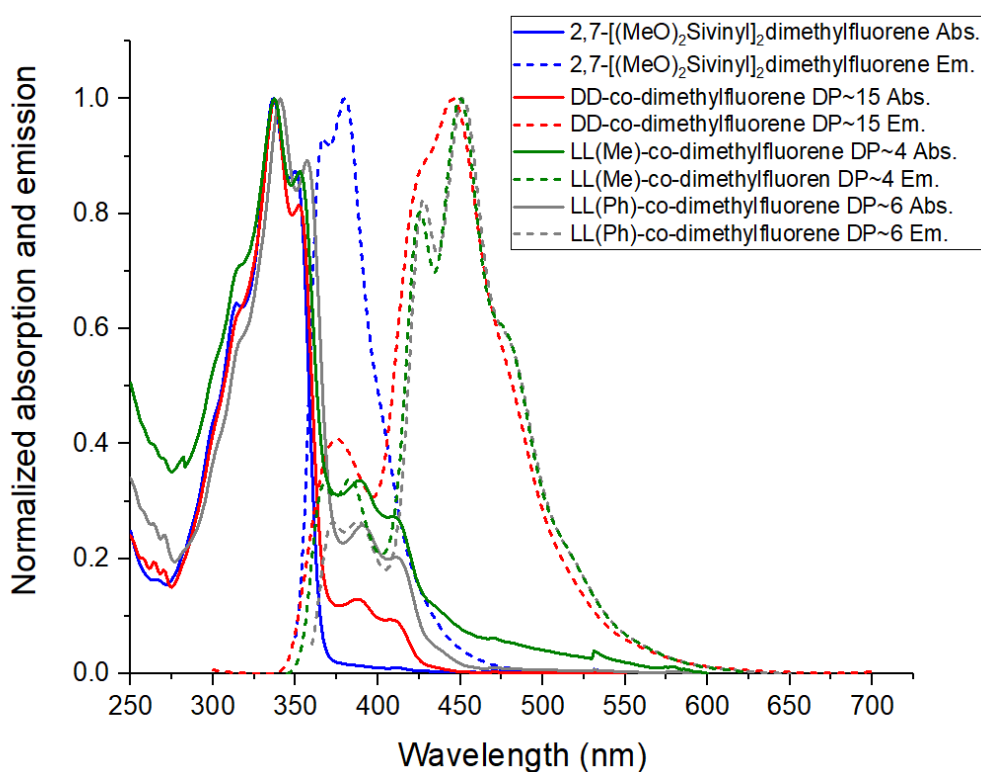

Figure S12. Normalized steady-state spectra of 2,7-[(MeO)$_2$Sivinyl]$_2$dimethylfluorene, DD-co-dimethylfluorene and LL(Me/Ph)-co-dimethylfluorene in CH$_2$Cl$_2$.
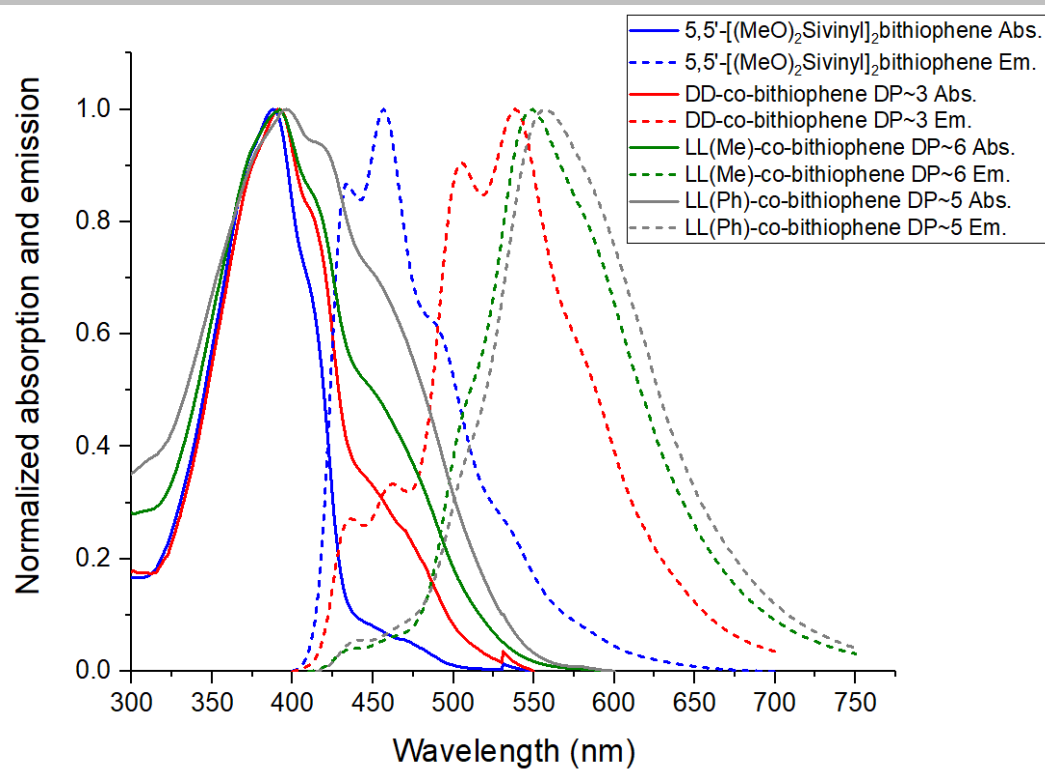
Figure S13. Normalized steady-state spectra of 5,5'-[(MeO)$_2$Sivinyl]$_2$bithiophene, DD-co-bithiophene and LL(Me/Ph)-co-bithiophene in CH$_2$Cl$_2$.
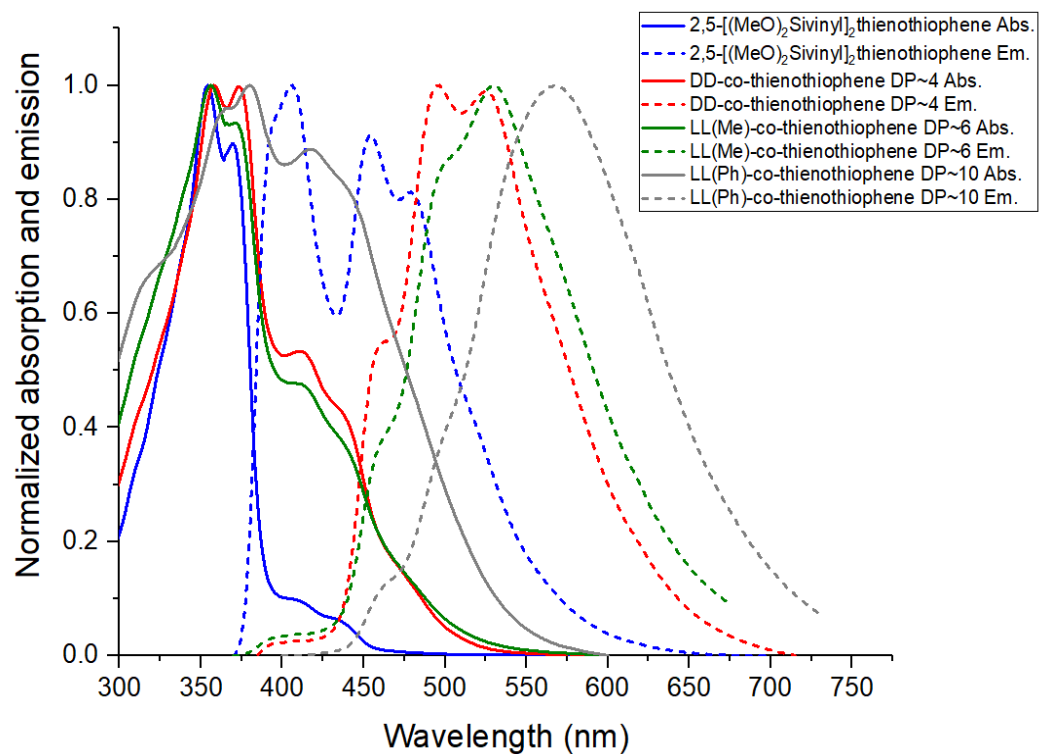
Figure S14. Normalized steady-state spectra of 2,5-[(MeO)$_2$Sivinyl]$_2$thienothiophene, DD-co-thienothiophene and LL(Me/Ph)-co-thienothiophene in CH$_2$Cl$_2$.
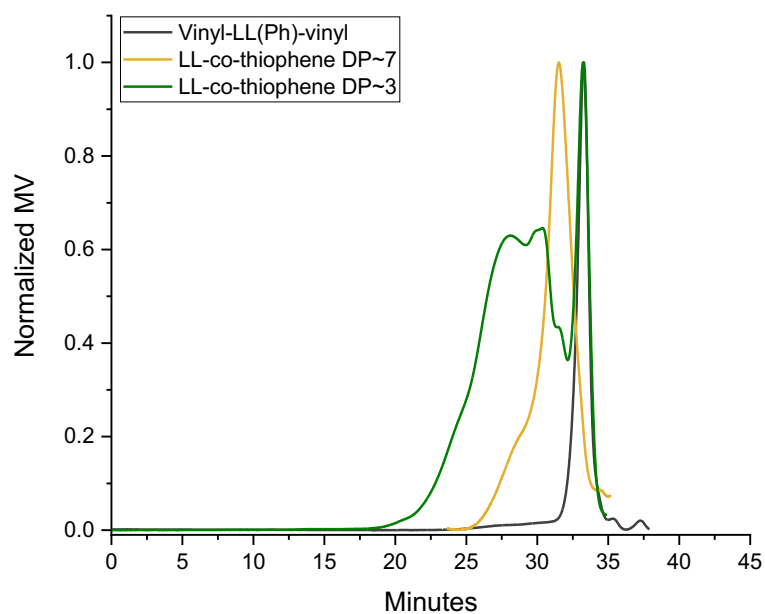
Figure S15. GPC of vinyl-LL-vinyl, short oligomers of LL-co-thiophene separate from TLC and long oligomers of LL-co-thiophene.
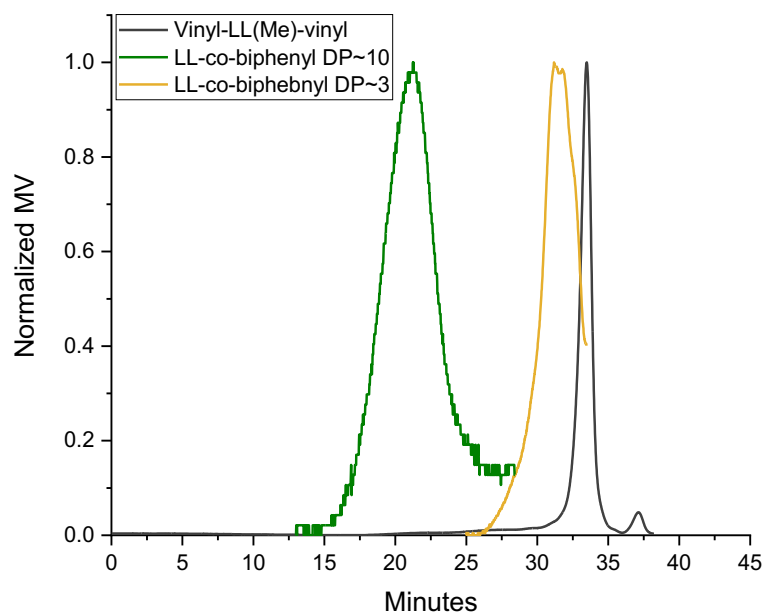
Figure S16. GPC of vinyl-LL-vinyl, short oligomers of LL-co-biphenyl separate from TLC and long oligomers of LL-co-biphenyl.
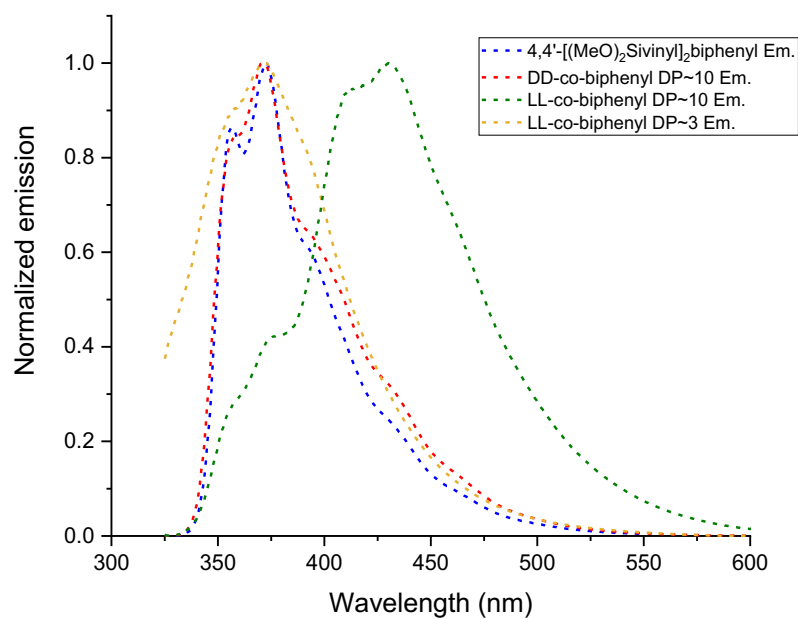
Figure S17. Normalized progressive emission spectra of 4,4'-[(MeO)$_2$Sivinyl]$_2$biphenyl, DD-co-biphenyl, short (DP~3) and long (DP~8) LL-co-biphenyl in CH$_2$Cl$_2$.

Analytical characterization of brominated and debrominated LL-co-phenyl.
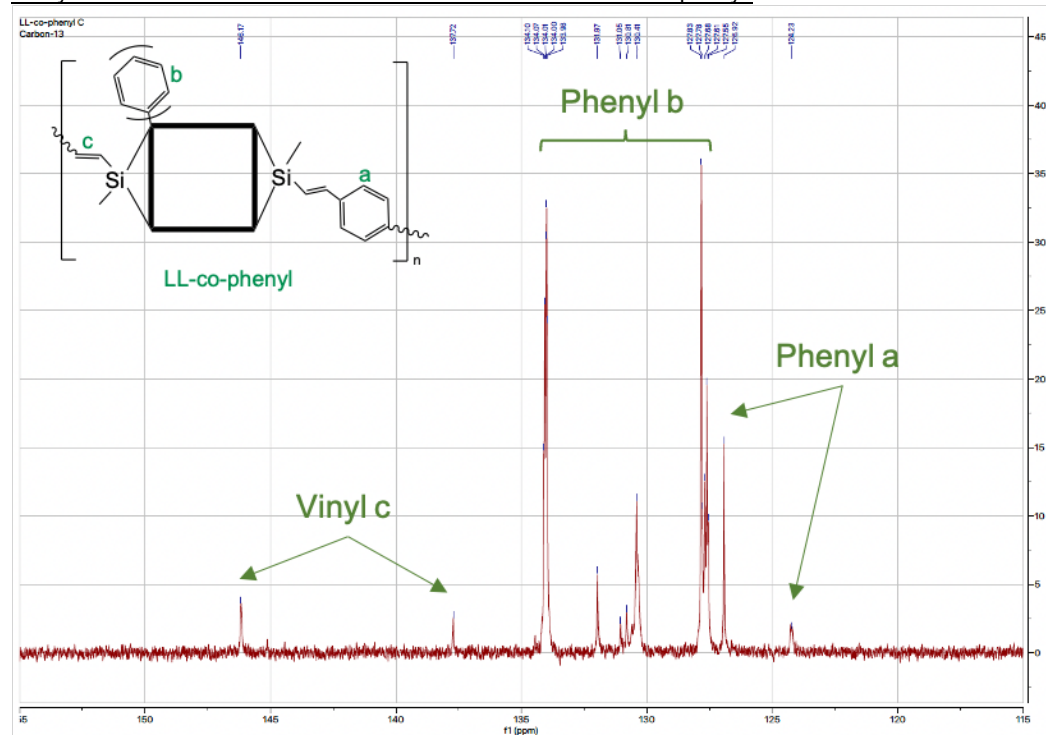
Figure S18. ^{13}C NMR of LL-co-phenyl (zoom-in).
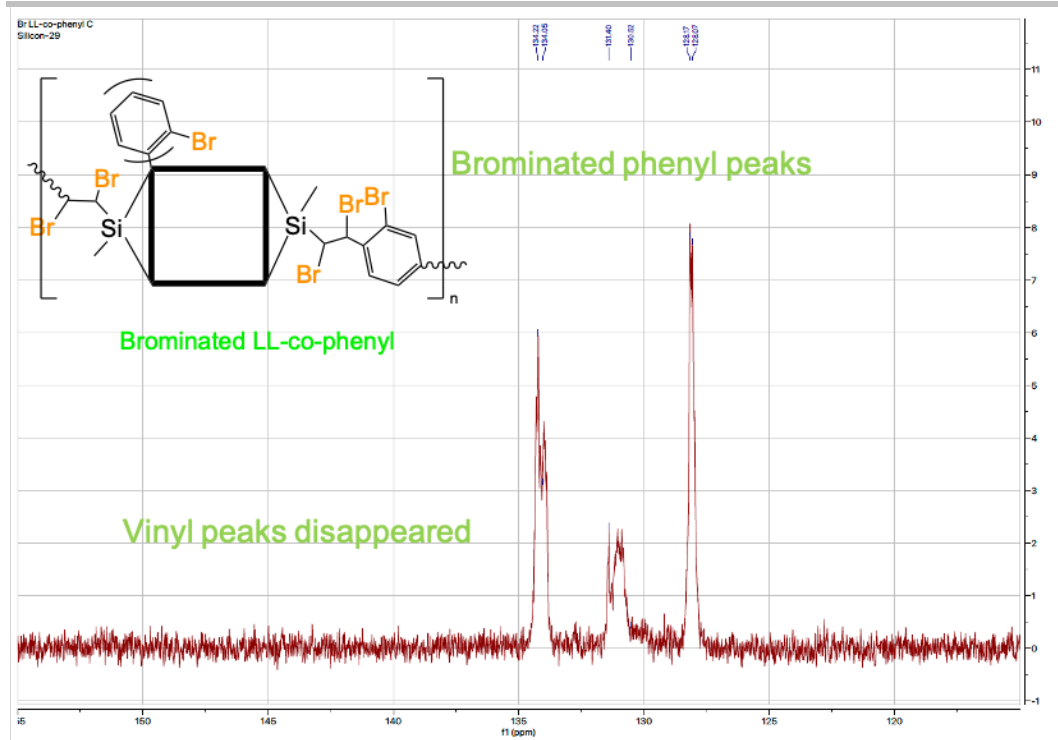
Figure S19. ^{13}C NMR of brominated LL-co-phenyl (zoom-in).

Analytical and photophysical characterization of brominated and debrominated DD-co-phenyl.
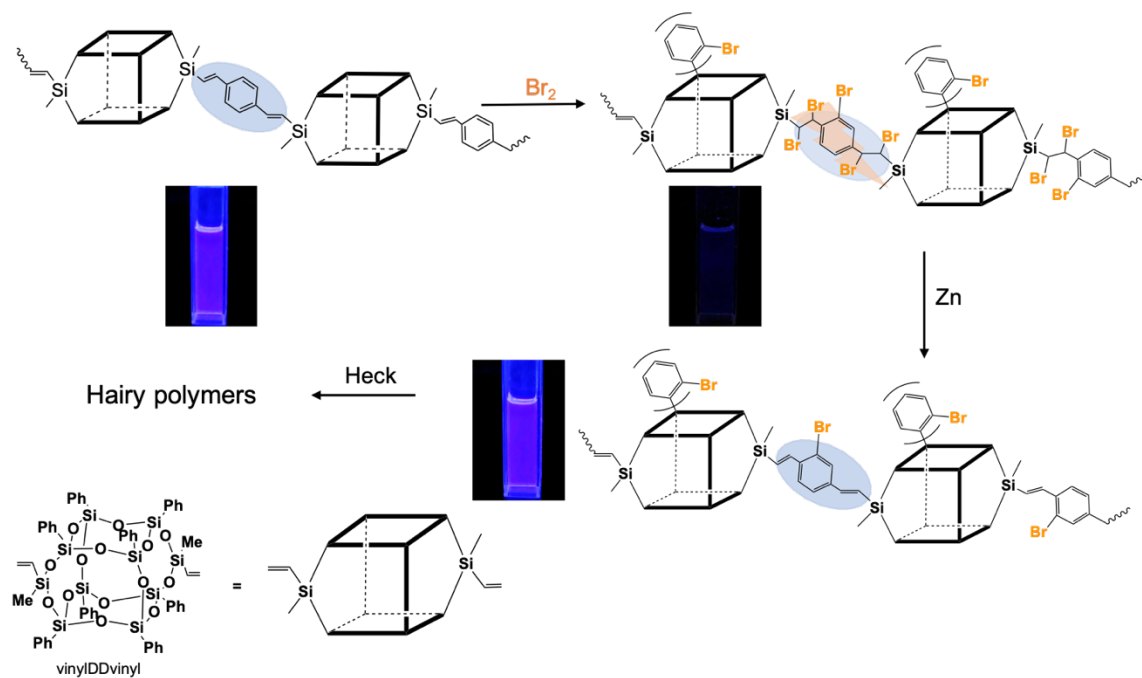
Figure S20. Bromination and debromination of DD-co-phenyl.
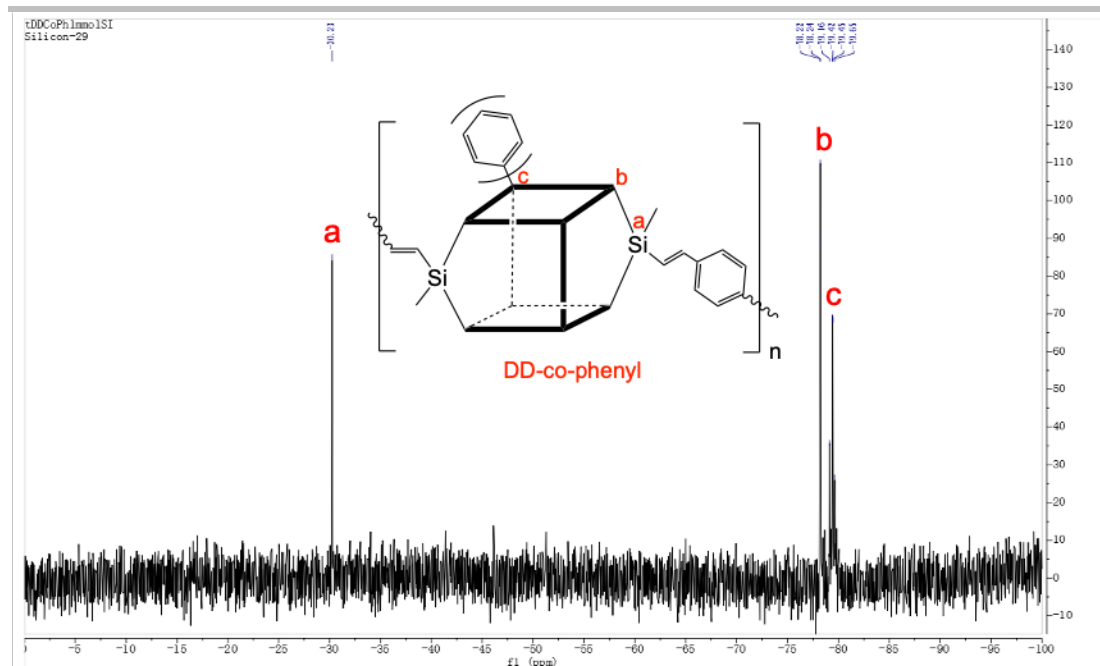
SUPPORTING INFORMATION
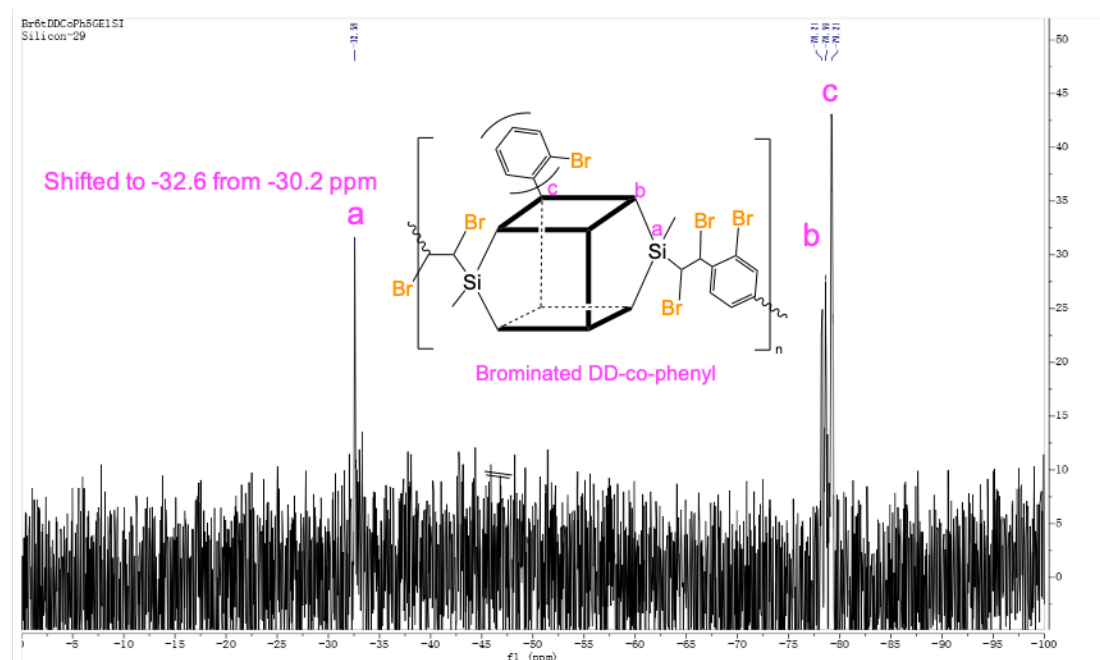

Figure S21. ^{29}Si NMR of DD-co-phenyl.

Figure S22. ^{29}Si NMR of brominated DD-co-phenyl.
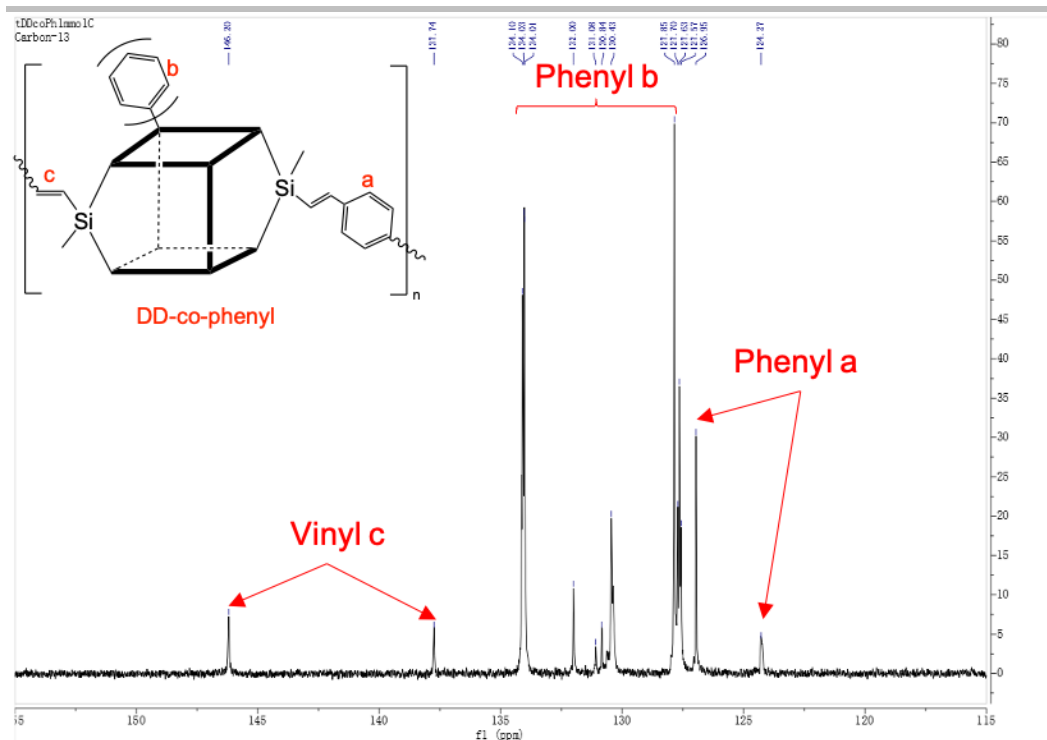
Figure S23. ^{13}C NMR of DD-co-phenyl (zoom-in).

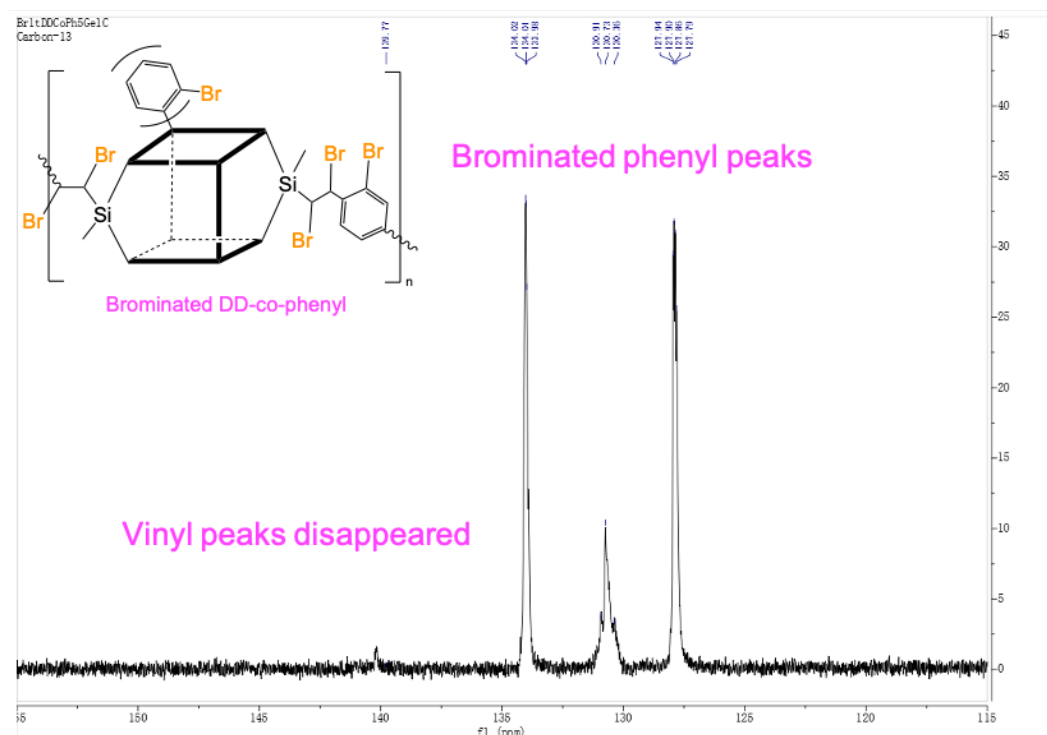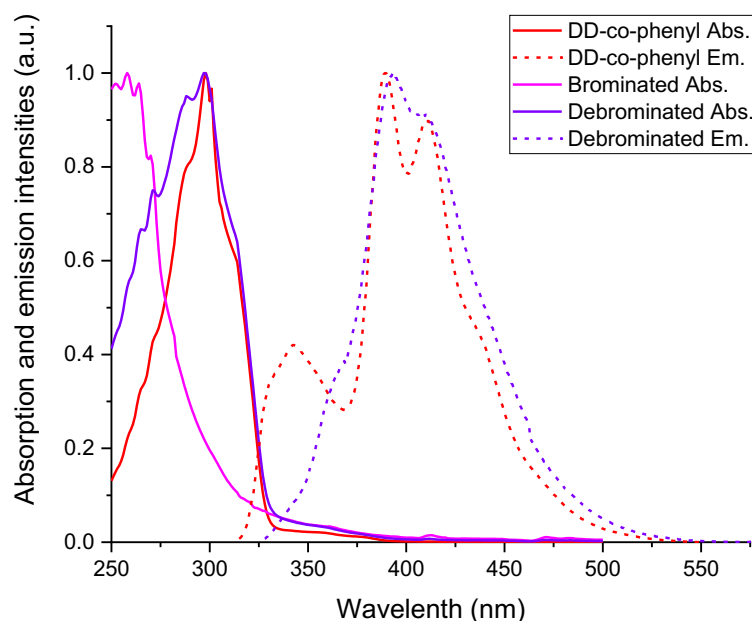**Figure S24**. ^{13}C NMR of brominated DD-co-phenyl (zoom-in).

Figure S25. Steady-state spectra of DD-co-phenyl, brominated and debrominated DD-co-phenyl in CH_2Cl_2.

Modeling.

Modeling of vinyl-LL(Me)-vinyl and vinyl-LL(Ph)-vinyl done by Professor Jungsuttiwong's group at Ubon Ratchathani University, Thailand are shown in Table **S4**. Modeling suggests LUMOs reside on phenyl groups and the calculated absorption λ_{max} is always blue-shifted from experimental by ~60 nm. One might choose to argue that current modeling methods are unable to successfully address the interaction of LL SQ centered LUMOs with conjugated moieties. Hence efforts to model the unique structures developed with the LL polymers wherein centered LUMOs must interact with co-monomer LUMOs through vinylMeSi(O-)$_2$ bridges (assuming our arguments are valid) must search for new modeling approaches.

**Table S4.** Experimental and modeling data for vinyl-LL(Me/Ph)-vinyl.

	Experimental Abs. λ_{max} (nm)	Modeling Abs. λ_{max} (nm)	Transition	HOMO (eV)	LUMO (eV)	E_{gap} (eV)
Vinyl-LL(Me)-vinyl	264	203	HOMO to L+1 (40%)	-8.07	0.81	8.88
Vinyl-LL(Ph)-viny	265	201	H+9 to L+2 (26%)	-8.28	0.72	8.99
		203	H+6 to LUMO (18%)	-8.32	0.80	9.13

Modeling indicates studies done on vinyl-LL(Me)-vinyl by Professor Kieffer and Dr. Hashemi's group at University of Michigan are shown in Figure **S26-28**. In these modeling studies, both *cis* and *trans* isomers have about the same energy, which may explain why it is always a mixture of *cis* and *trans*. The energy of *cis* isomer is ~0.025 eV slightly lower than *trans*. Additionally, there are two different conformation, chair and boat conformation as shown in Figure **S26**, similar to cyclohexane. The chair conformation is more stable with the energy difference of ~0.13 eV. What's more important is that LUMO+2 at 8.47 eV is from LL SQ core and extends out of the ladder structure in Figure **S27**, which makes interaction between SQ-centered LUMO and vinyl π* possible. Phenyl groups are replaced by methyl for modeling. When phenyl unreplaced, LUMO+10 is from LL SQ core with energy level at 7.86 eV as shown in Figure **S28**, which has a lower energy level than LUMO+2 of methyl-replaced model.
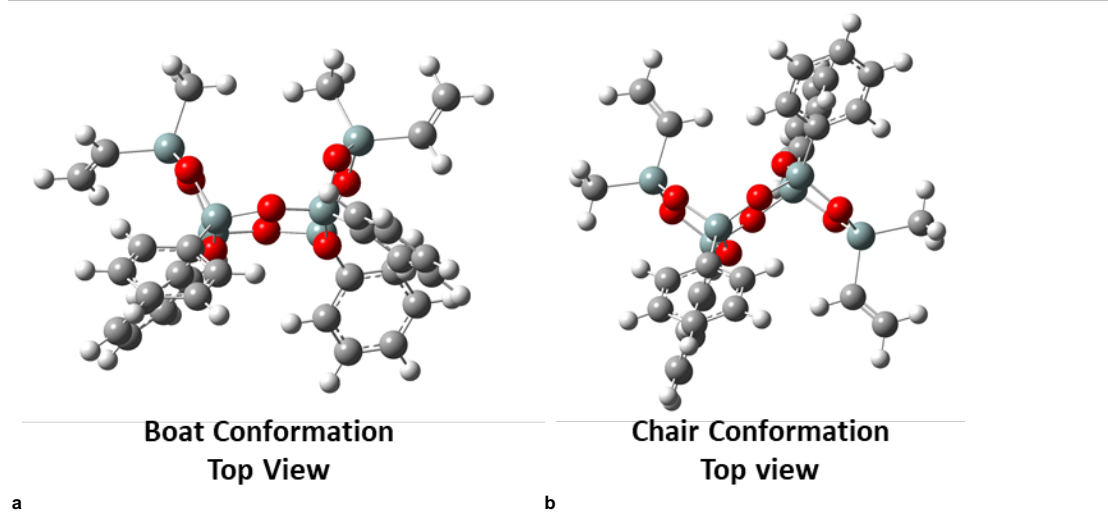
Figure S26. (a) boat conformation of *trans*-vinyl-LL(Me)-vinyl, (b) chair conformation, calculated at B3LYP/6-31G(d,p) level.
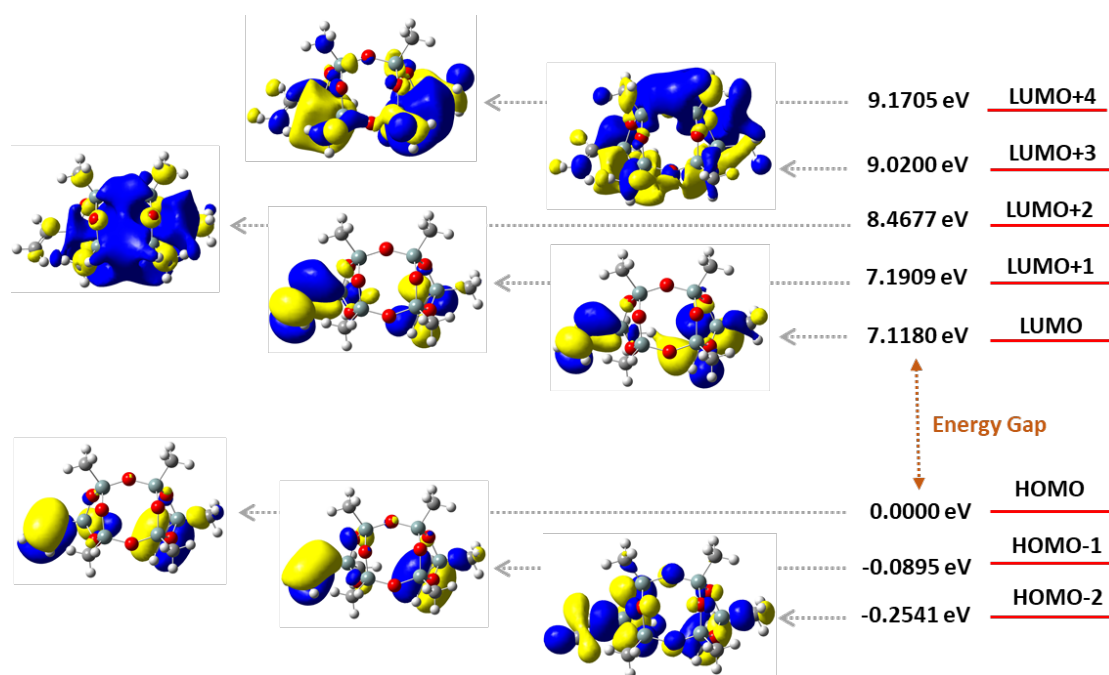
Figure S27. Energy diagram of the molecular orbitals of methyl substituted vinyl-LL(Me)-vinyl.
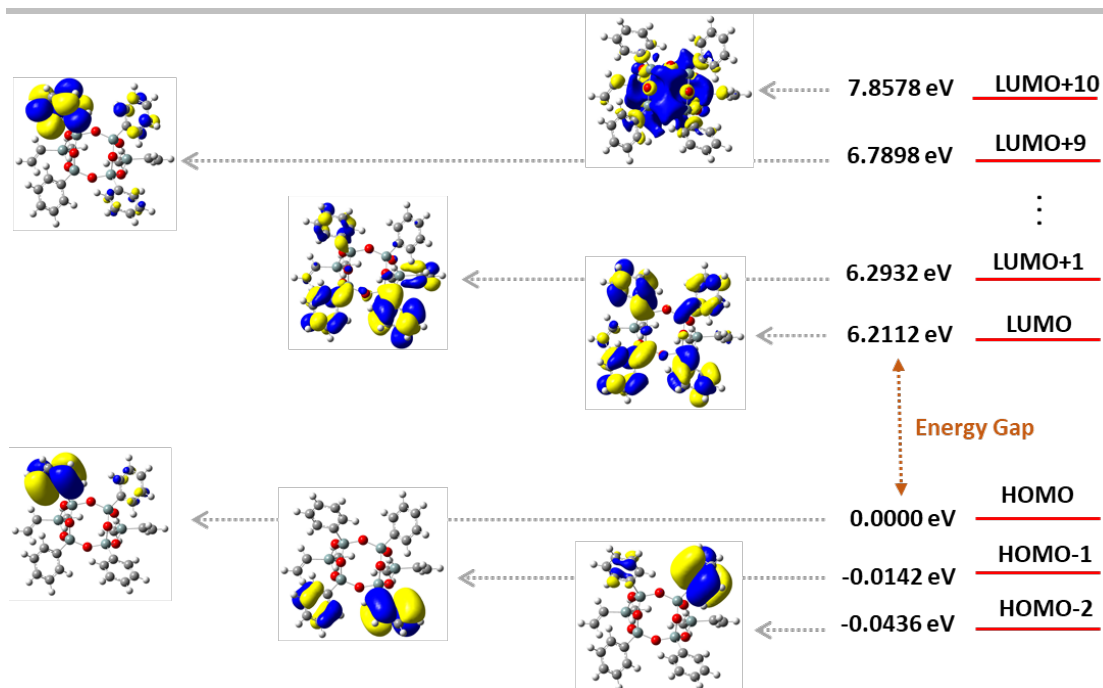
Figure S28. Energy diagram of the molecular orbitals of vinyl-LL(Me)-vinyl.

References

[1]   Guan, J.; Arias, J. J. R.; Tomobe, K.; Ansari, R.; Marques, M. de F. V.; Rebane, A.; Mahbub, S.; Furgal, J. C.; Yodsin, N.; Jungsuttiwong, S.; Hashemi, D.; Kieffer, J.; Laine, R. M. Unconventional Conjugation via VinylMeSi(O−)$_2$ Siloxane Bridges May Imbue Semiconducting Properties in [Vinyl(Me)SiO(PhSiO$_{1.5}$)$_8$OSi(Me)Vinyl-Ar] Double-Decker Copolymers. *ACS Appl. Polym. Mater.* **2020**, *2* (9), 3894–3907.

[2]   Guan, J.; Tomobe, K.; Madu, I.; Goodson, T.; Makhal, K.; Trinh, M. T.; Rand, S. C.; Yodsin, N.; Jungsuttiwong, S.; Laine, R. M. Photophysical Properties of Partially Functionalized Phenylsilsesquioxane: [RSiO$_{1.5}$]$_7$[Me/NPrSiO$_{1.5}$] and [RSiO$_{1.5}$]$_7$[O$_{0.5}$SiMe$_3$]$_3$ (R = 4-Me/4-CN-Stilbene). Cage-Centered Magnetic Fields Form under Intense Laser Light. *Macromolecules* **2019**, *52* (11), 4008–4019.

[3]   Brook, A. G.; Duff, J. M.; Reynolds, W. F. The Bromination, Debromination and Debromosilylation of Silylstyrenes and Other Vinylsilanes. *Journal of Organometallic Chemistry* **1976**, *121* (3), 293–306.

[4]   Kresse, G.; Hafner, J. *Ab Initio* Molecular-Dynamics Simulation of the Liquid-Metal–Amorphous-Semiconductor Transition in Germanium. *Phys. Rev. B* **1994**, *49* (20), 14251–14269.

[5]   Kresse, G.; Furthmüller, J. Efficiency of Ab-Initio Total Energy Calculations for Metals and Semiconductors Using a Plane-Wave Basis Set. *Computational Materials Science* **1996**, *6* (1), 15–50.

[6]   Perdew, J. P.; Burke, K.; Ernzerhof, M. Generalized Gradient Approximation Made Simple. *Phys. Rev. Lett.* **1996**, *77* (18), 3865–3868.

[7]   Blöchl, P. E. Projector Augmented-Wave Method. *Phys. Rev. B* **1994**, *50* (24), 17953–17979.

[8]   Kresse, G.; Joubert, D. From Ultrasoft Pseudopotentials to the Projector Augmented-Wave Method. *Phys. Rev. B* **1999**, *59* (3), 1758–1775.

[9   Tkatchenko, A.; DiStasio, R. A.; Car, R.; Scheffler, M. Accurate and Efficient Method for Many-Body van Der Waals Interactions. *Phys. Rev. Lett.* **2012**, *108* (23), 236402.

[10]   Momma, K.; Izumi, F. *VESTA 3* for Three-Dimensional Visualization of Crystal, Volumetric and Morphology Data. *J Appl Crystallogr* **2011**, *44* (6), 1272–1276.